IEEE Transactions on Nuclear Science, Vol.NS-22, No.3, June 1975

SINGLE PARTICLE AND COLLECTIVE EFFECTS OBSERVED IN THE ELECTRON BEAM OF THE MARYLAND ERA EXPERIMENT*

W. W. Destler, D. W. Hudgings, R. A. Kehs,
P. K. Misra and M. J. Rhee

University of Maryland
College Park, Maryland 20742

Abstract

The formation of rotating, relativistic electron beams with properties suitable for collective ion acceleration has been studied under a variety of experimental conditions. A straight, cylindrical, relativistic electron beam (typical energy 2-3 MeV, typical current 2-10 kA) is passed through a narrow magnetic cusp, and the resulting rotating downstream beam has been studied using a number of diagnostic techniques. Two current regimes have been investigated: one in which the self-fields of the downstream electron beam are small compared to the applied fields, and one in which the self-fields are comparable to the applied fields. The beam characteristics in both regimes have been compared to single particle expectations. Experiments have also been conducted in which the effect of an inner and outer conducting boundary on the time-resolved beam cross section has been measured. Results will be discussed in the context of collective ion acceleration experiments now in preparation.

I. Introduction

The basic concept behind the electron ring accelerator involves the trapping of a number of positive ions in the potential well of a dense relativistic electron ring. As long as the number of trapped ions is only a small fraction of the number of electrons in the ring, the ion-loaded ring may be accelerated to high velocity using externally applied electric or magnetic fields.

The most important goal, therefore, is the creation of an electron ring of sufficiently high density that the maximum electric field strength at the surface of the ring is great enough to be reasonably attractive for collective ion acceleration experiments. A reasonable estimate of this "holding power" of an electron ring of elliptical cross section is given by:[1]

$$E_{max} = \frac{9.2 \times 10^{-12} N_e}{R_{[cm]}(a+b)_{[cm]}} \left[\frac{MV}{m}\right] \qquad (1)$$

where N_e is the total number of electrons in the ring, R is the major radius of the ring, and a and b are the semi-axes. As an example, if a ring could be formed of 10^{13} electrons, with R = 6 cm and a + b = 1 cm, then E_{max} = 15.3 MV/m. The condition for acceleration of positive ions trapped in such a potential well is that the effective external accelerating field must be smaller than the holding power of the ring. A detailed analysis of possible acceleration mechanisms has been reported previously.[2,3]

In this paper, experiments are reported in which hollow, rotating relativistic electron beams are generated by passing a hollow, non-rotating, relativistic electron beam through a narrow magnetic cusp and then into a downstream drift region. Measurements of the self-magnetic fields, axial velocity, and time-resolved cross section of the downstream electron beam have been made under a variety of experimental conditions, and these results will be discussed in the context of desirable electron ring parameters for collective ion acceleration.

II. Experiments

The experiments were performed in the cusped magnetic field of the University of Maryland Electron Ring Accelerator Project, shown schematically in figure 1. In the experiment, two opposing solenoids are used to form a magnetic cusp, and the downstream solenoid is extended to provide a drift region in which the particle motion is essentially adiabatic. The transition width of the cusp is narrowed substantially by a soft iron plate placed between the solenoids. Measurements of the axial and radial magnetic field components through the cusp region indicate that the effective cusp transition width is about 1.5 cm. A hollow, relativistic electron beam is emitted from a circular knife-edge cathode approximately 10 cm upstream of the cusp transition. The radius of the cathode knife-edge is 6 cm. An aluminum or brass plate attached to the surface of the iron plate serves as the anode. The cusp field is sufficiently narrow that the electron motion is essentially non-adiabatic and the electrons see primarily the $v_z \times B_r$ force in the transition region. This force acts to convert the axial beam velocity on the diode side of the cusp into rotational velocity on the downstream side. The electrons pass through an annular slit in the iron plate and the effective area of the slit can be varied to achieve some control over the total current propagating into the downstream region. Typical diode voltages and currents are 1-3 MV and 4-20 kA, respectively. The magnitude of the magnetic field on the diode side at z = - 10 cm was set equal to that on the downstream side at z = +10 cm. The pulse width at half maximum of the electron beam on the diode side may be controlled by a peaking switch in the transformer section. For the experiment reported here, it was about 20 ns. The experiments were performed at sufficiently good vacuum (about 10^{-5} torr) that charge neutralization of the electron beam is negligible both upstream and downstream of the cusp transition.

The downstream beam propagates within a drift tube one meter in length and 15 cm in inner diameter, as shown in figure 1. A squirrel cage inner conductor of outer radius 4 cm, designed to provide an inner conducting boundary without azimuthal image currents, can be inserted from the downstream end of the drift tube. Beam propagation characteristics have been measured both with and without the squirrel cage.

A. Measurements of the Downstream Beam Self-Magnetic Field.

An important indication of the current density J_Θ in a hollow, rotating electron beam is the peak axial self-magnetic field on axis. Very fast (< 1 ns rise-time) integrated $\dot{B}$ loops have been used to measure the self-B_z of the downstream beam under a variety of experimental conditions. Variation of the total current entering the downstream drift region can be achieved by changing the effective area of the annular slit in the iron plate through which the beam passes. Figure 2 shows plots of the self-B_z of the

downstream beam as a function of applied magnetic field B_o for three different effective slit areas. The 100% transmission anode corresponds to a 0.5 cm wide annular slit centered about the 6 cm cathode radius. It can be seen that, while the highest self-fields are measured when the 100% transmission anode is used, peak self-fields measured using the 40% transmission anode are only slightly less. It is this 40% transmission anode configuration that has produced the best combination of total beam current, axial and radial confinement, and pulse duration on the downstream side of the cusp, and the remaining data presented in this paper was taken using this anode.

A plot indicating the effect of the squirrel cage inner conductor on the beam self-fields is shown in figure 3. It is easily seen that significantly higher self-fields are measured when the squirrel cage is in place.

B. Time-Resolved Measurements of the Downstream Beam Cross Section.

Figure 4 shows the experimental configuration used for the time-resolved study of the downstream beam cross section. The electron beam travels a distance z_o downstream of the cusp transition and strikes a thin scintillating rod. The scintillation light from this rod is photographed with the use of an image converter camera operating in the streak mode. A typical streak photograph is also shown in the figure.

Single particle theory[4] predicts that the axial velocity v_{z_2} of an electron on the downstream side of an ideal cusp can be written in terms of the upstream velocity v_{z_1} as:

$$v_{z_2}^2 = v_{z_1}^2 - r_o^2\omega_c^2 \qquad (2)$$

where r_o is the major radius of the electron beam and ω_c is the relativistic electron cyclotron frequency. Thus there exists a threshold electron energy below which electrons will be reflected at the cusp. This threshold energy for electrons is, in laboratory units:

$$E_{th}(\text{MeV}) = [0.261+8.989\text{x}10^{-2}r_o^2B^2]^{1/2}-0.511 \qquad (3)$$

with units of r_o and B in cm and kilogauss, respectively. This reflection of lower energy electrons should result in a narrowing in time of the current pulse downstream of the cusp, since those electrons accelerated during the leading and trailing edge of the diode voltage waveform will be reflected. The duration of the downstream beam as measured from the streak photographs of the beam cross section has been plotted as a function of applied magnetic field B_o in figure 5. Data is shown for beams propagating with and without the squirrel cage inner conductor, and can be compared with the result expected from the single particle theory. It can be seen that the best agreement with theoretical expectations is found for the case where the beam propagates with the squirrel cage in place. Agreement between these results and those obtained from the self-B_z waveforms is excellent.

These measurements have also been used to construct the plot of downstream beam half-width R_b as a function of applied magnetic field shown in figure 6. This downstream beam width has been measured at the point in time when the self-magnetic field of the beam measured at the same axial position was a maximum. It can be seen that the presence of the squirrel cage inner conductor greatly reduces the radial blow-up of the beam at high values of applied magnetic field.

C. Axial Velocity Measurements.

A rough estimate of the axial velocity of the downstream beam has been obtained using the technique shown schematically in figure 7. The beam travels a distance z_o downstream of the cusp transition and strikes a graphite covered Plexiglas plate. Cherenkov radiation produced from electron impact in the Plexiglas is photographed from the downstream end of the vacuum chamber. The shadow cast by a radial flag on the surface of the plate is used to determine the maximum β_z of the electrons in the beam. A typical photograph is also shown in the figure.

Experimentally, the axial velocity can be found from:

$$\beta_z = \frac{h}{c}\frac{eB}{m\gamma\Theta} \qquad (4)$$

where h is the height of the flag above the surface of the Plexiglas plate. Using equation (2), the predicted shadow angle cast by the flag can be written:

$$\Theta = \frac{heB}{cm\gamma}\left[\frac{1}{1-\dfrac{r_o^2e^2B^2}{m^2\gamma^2c^2}}\right]^{1/2}$$

Figure 8 shows a plot of β_z as a function of applied magnetic field measured in this manner, and can be compared to the theoretical curve for $\gamma = 4.79$. The axial velocity of the downstream beam agrees with theoretical expectations down to a β_z of about 0.1. Power supply regulation problems have made measurements of even lower values of β_z difficult, since a change in applied field of only 7 gauss can make the difference between $\beta_z = 0$ and $\beta_z = 0.1$. Work on these problems is currently underway and at this point there appears to be no inherent problems in reducing β_z to values significantly below 0.1.

III. Conclusions

The measurements presented in section II can be used to construct a reasonable model of the downstream beam from which an estimate of the holding power of the beam can be obtained. The radial width of the beam can be measured directly from the streak photographs of the downstream beam cross section. The axial length of the downstream beam can be obtained from the streak duration τ_s and the axial velocity measurements. The total current in the beam can be estimated by assuming the downstream beam to be an ideal solenoid of length L and radius R = 6 cm with a peak self-magnetic field on axis as measured experimentally. Thus, if wall effects are ignored, the total azimuthal current in the beam can be estimated from:

$$I_\Theta = \frac{2}{\mu_o}\left[R^2 + \frac{L^2}{4}\right]^{1/2} B_{z_{self}} \qquad (6)$$

The total number of electrons in the beam N_e can be obtained from this result by noting that:

$$N_e = \frac{I_\Theta \tau_c}{e} \qquad (7)$$

where $\tau_c = \frac{2\pi}{\omega_c}$. Typical experimental numbers are $\tau_s = 3$ ns, $\beta_z = 0.1$, $B_{z_{self}} = 300$ gauss, $\tau_c = 1.3$ ns,

and R_b = 0.5 cm. Thus L = 9 cm and N_e = 3.0 x 10^{13}. Under these conditions, E_{max} is about 9.2 MV/m. By reducing β_z from 0.1 to 0.02 through careful control of the magnetic field, the length L is compressed by a factor of 5 and E_{max} will increase to approximately 45 MV/m. If the effect of the outer conducting boundary is considered, the holding power calculated in this manner should be enhanced. Holding powers in the range of 10 MV/m and above are quite reasonable for initial collective ion acceleration experiments.

Further experiments are planned in an attempt to reduce β_z to a value attractive for ion loading. An extension of the downstream field to provide a suitable expansion-acceleration region is currently under construction. In addition, design and construction of a fast-trapping coil system[5] is underway. This system will actually stop ($\beta_z \simeq 0$!) the electron beam for a short period of 100 to 200 ns where ion loading takes place before the ring is released for expansion-acceleration.

References

1. M. P. Reiser, IEEE Trans. NS-19, 280 (1972).

2. M. P. Reiser, Netherlands Journal of Natural Sciences 38, 219 (1972).

3. D. Keefe, Particle Accelerators, Vol. 1, No. 1 (1970).

4. M. J. Rhee and W. W. Destler, Phys. Fluids 17, 1574 (1974).

5. M. P. Reiser, IEEE Trans. NS-20, 310 (1973).

*Research supported by the National Science Foundation.

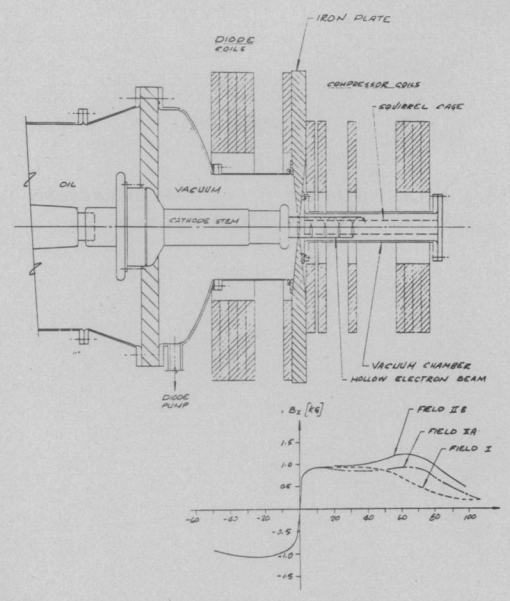

Fig. 1. Diode and Magnetic Field Geometry.

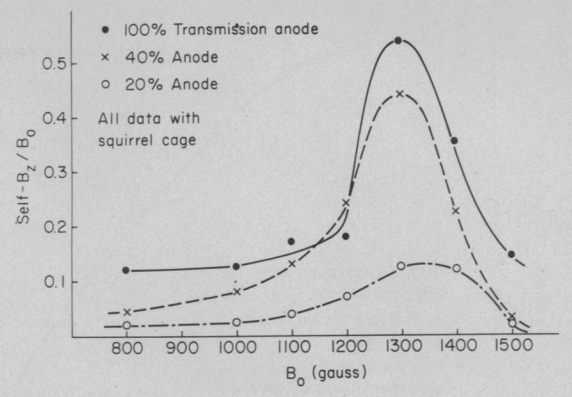

Fig. 2. Self-magnetic field on axis (normalized to applied field B_0) for three different effective anode slit areas.

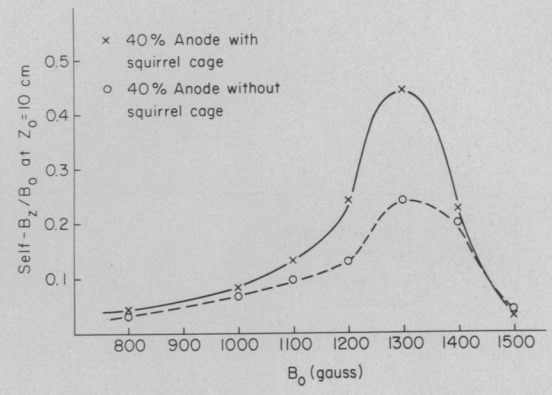

Fig. 3. Self-magnetic field on axis (normalized to B_0) with and without squirrel cage innter conductor.

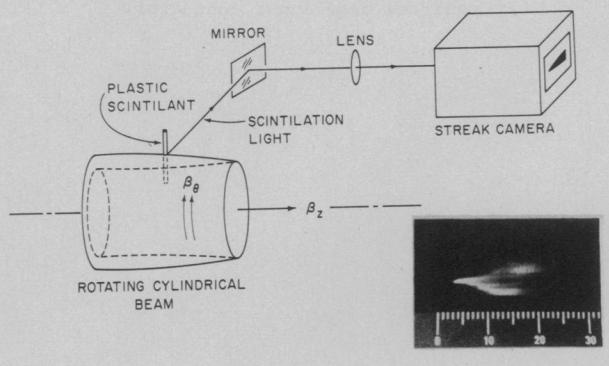

Fig. 4. Experimental configuration used for the time resolved measurements of the downstream beam cross section.

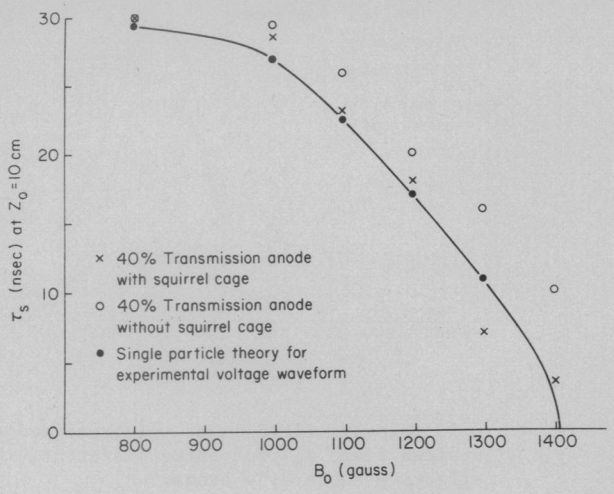

Fig. 5. Streak duration τ_s versus applied field B_o with and without the squirrel cage inner conductor.

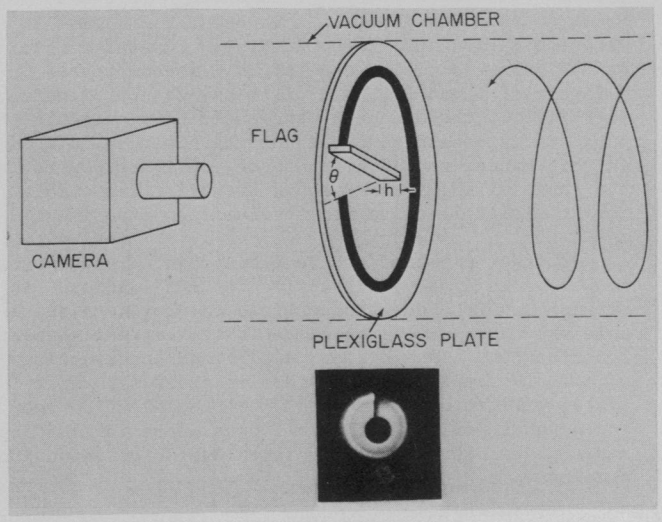

Fig. 7. Experimental configuration used for the measurements of the axial velocity of the downstream beam.

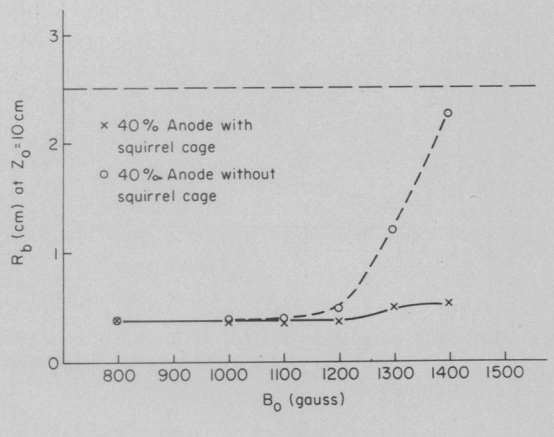

Fig. 6. Downstream beam radial half-width R_b versus applied field B_o with and without squirrel cage inner conductor.

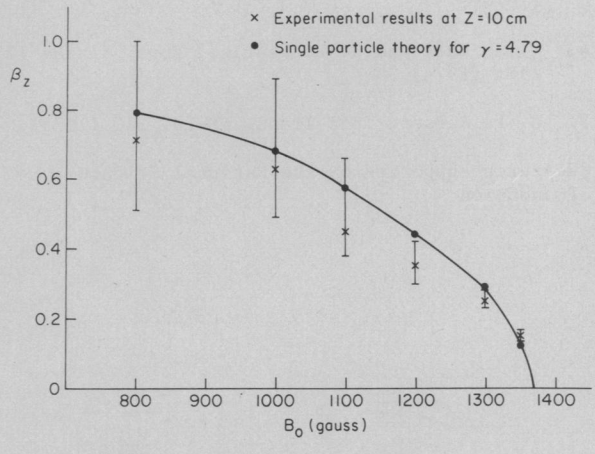

Fig. 8. Axial velocity β_z of the downstream beam versus applied field B_o.